UNH-71-15

FIELD LINE MOTION DURING GEOMAGNETIC STORMS

Richard L. Kaufmann and Jiann-Tsorng Horng

Department of Physics

University of New Hampshire, Durham, 03824

and

Andrei Konradi

NASA/Manned Spacecraft Center

Houston, Texas, 77058

ABSTRACT

We have found that the high-latitude trapping boundary for 20-kev electrons and 100-kev protons becomes very thin in the early morning hours during two intense substorms. The gradients are too steep to be maintained by drifting particles, so they must be produced locally over the night side of the earth. The flux gradient is seen to move at speeds in excess of 100 km/sec. Plasma appears to move away from the tail and around the earth at these high speeds during the sudden expansion phases of the substorms. The rapid plasma motion requires the presence of 50 to 100 mV/m electric fields at a geomagnetic latitude of 30° on the L=5 field line. Our observations fit best into a model that contains two field-aligned sheet currents. Current flows downwards toward the ionosphere at or beyond the poleward edge of the disturbance, and away from the earth at lower latitudes. The high-latitude trapping boundary appears to be distorted by waves. As these waves propagate around the earth, the satellite alternately enters and leaves the trapped particle region. Electrons that have been newly accelerated during the substorm arrive at the satellite at about the same time that ground activity commences at the satellite's local time. The high electric fields that accompany the rapid plasma flow can produce non-adiabatic

acceleration of 0.1 to 1 Mev electrons and protons.

A SSC event is also observed near dawn. The event appears to be produced by an increase in the viscous drag at the magnetopause and an increase in the total pressure on the magnetopause. Three MHD waves are excited by the SSC: a compressional pulse that propagates across field lines to equatorial ground stations, a field-line distortion that propagates along field lines to auroral stations, and a torsional oscillation that is confined to equatorial regions.

INTRODUCTION

Many current models of substorms suggest that the sudden expansion phase is associated with a sudden collapse of the geomagnetic tail. It is often assumed that plasma pressure at the base of the tail suddenly decreases, and that it is this pressure decrease that allows the tail to collapse. Explorer 12 is able to measure energetic particles and magnetic fields down to 3 earth radii, so is well adapted to a study of the base of the tail. In this paper, we present evidence that plasma begins flowing rapidly away from this region during, or slightly before, the sudden expansion phases of two intense substorms. This rapid flow may play an important role in producing the pressure decrease that initiates the substorm expansion.

We also present data from one large SSC event that occurred when the sate-lite was at L=8 near the geomagnetic equator. The initial magnetic field and particle flux changes fit a simple model involving an increase in the pressure on the magnetopause and an increase in the drag of field lines into the tail. Torsional oscillations of the outer magnetosphere are set up by the SSC. The observed perturbations appear to be produced by three separate MHD waves.

The data used are from ground magnetograms, and from the Explorer 12 magnetometer (Cahill and Amazeen, 1963), ion-and-electron detector (Davis and Williamson, 1963), and cadmium sulfide detectors (Freeman, 1964). By combining these data, we are able to study field distortions, to measure particle flux gradients, and to determine the speed at which these flux gradients move past the satellite.

The substorm-associated events that we investigated have already been studied by Konradi (1968) using ion-and-electron detector data and by Yeager and Frank (1969) using data from arrays of Geiger-Mueller tubes. We selected these same events because they are the only ones available that involved extremely rapid flux changes. Rapid flux changes are needed in order to measure the flux gradient with a single satellite. In the previous studies, Konradi (1968) concluded that the sudden flux changes could not be produced by the motion of the satellite from one stable drift shell that contained large energetic particle fluxes to another stable shell that was void of energetic particles. He therefore concluded that some temporal change in the particle fluxes is required. Yeager and Frank (1969) studied two of the Explorer 12 events and several additional rapid flux changes seen by Explorer 14. They concluded that the rapid flux changes could be produced by the motion of the high-latitude trapping boundary past the satellite as

the magnetosphere is inflated or compressed.

The addition of magnetometer data to the energetic particle flux measurements leads us to propose that most of the plasma motion is around the earth in longitude rather than radially toward or away from the earth. We also observe very steep energetic particle flux gradients that are produced over the night side of the earth. These gradients occasionally move at speeds of at least 100 km/sec near the equator. Such rapid motion requires the presence of very large electric fields, and these fields can play an important role in the acceleration of energetic particles during substorms.

OBSERVATIONS

Structure of the substorm events on a 5-second time scale. Figure 1 shows magnetic field and energetic electron data for the October 27 event. The ion-and-electron detector samples electrons with energies in a given band three times per second for about 5 seconds, and then switches to a different energy range. Most electrons detected have energies between 20 kev and 100 kev. One entire scan through all energy ranges is completed in 80 seconds. The electron fluxes shown in Figure 1 are the maximum fluxes seen during each 5-second interval. The maximum flux is usually seen when the detector looks at locally mirroring electrons.

The maximum fluxes in various energy bands have been normalized to the flux that would be seen in the most sensitive detector configuration. The normalization procedure assumes that the electron energy spectrum remains fixed during the interval of interest. This assumption is reasonably well met until 03:25, and it can be seen that there is not much point-to-point scatter before this time. Normalization produces an artificial point-to-point scatter when the flux rises after the 03:25 dropout, indicating that the electron energy spectrum has changed considerably at this time. No real wave structure or rapid time fluctuations were seen

after 03:25. An inspection of the available electron energy channels shows that the spectrum is much harder after the 03:25 dropout. Electron fluxes continue to rise until 03:35 when they peak and then drop to a level a little higher than that present at 03:30 (Konradi, 1968).

Fluxes of protons with energies >100 kev were also measured during the interval shown in Figure 1. On the 5-second time scale shown, the proton fluxes follow the electrons quite closely until 03:25 (Konradi, 1968). Some differences between changes in electron and proton fluxes were observed on a shorter time scale, and are illustrated in later figures. After 03:25, the hard electron flux became so intense that electron pulse pileup produced spurious counts in the proton channel. No reliable proton data are available after 03:25.

We believe that the electrons that begin to arrive at 03:25 are accelerated during the substorms and have just reached the satellite. Protons probably do not reach the satellite until later because they must drift around the earth. These conclusions are quite similar to those of Brown, et al. (1968) who observed a substorm on nearly the same L-shell, but on the dusk side of the earth. At that local time, newly accelerated protons were seen first, and electrons arrived after about one drift period.

The middle portion of Figure 1 shows the magnetic field magnitude, inclination, and declination, minus the

theoretical values of these quantities as computed using the Jensen and Cain (1962) model. Mead and Cahill (1967) discussed the usefulness of these angles in studying field distortions within the magnetosphere. They also noted that the absolute values of the angles measured by Explorer 12 could be in error by about 10 degrees, while short-term changes in these angles are accurately measured.

The declination angle is the only magnetic field parameter that is clearly connected with flux changes. McPherron and Coleman (1970) have also noted sudden changes in the declination angle at the synchronous altitude during substorms. We see that the declination is more negative than predicted by theory before the first dropout at 03:13. The satellite is after local midnight, and is south of the geomagnetic equator (Table 1) during this interval, so that a negative declination is expected when the solar wind exerts a viscous drag on field lines at the magnetopause and pulls them back into the tail. This is the distortion that is usually seen in the outer magnetosphere (Fairfield, 1968). At the start of each dropout event, the declination suddenly becomes more positive by 10° to 15°. This change suggests that the equatorial portions of field lines are suddenly moving from the tail toward the sun.

There is not a clear one-to-one correspondence between dropouts and changes in field inclination. Negative

changes in inclination are produced at the satellite location when field lines are pulled away from the earth at the equator. Field lines are stretched out during the 03:25 flux dropout, and relax when the new spectrum of hard electrons appears.

The only clear correlation between the field magnitude and particle fluxes is again seen during the 03:25 dropout. Positive changes in B indicate that the field is being locally compressed. Diamagnetic effects are expected to produce some local compression of the magnetic field whenever particle fluxes decrease.

The cadmium sulfide detector responds to both electrons and protons with energies greater than several hundred electron volts (Freeman, 1964). Figure 1 shows that the CdS flux decreases whenever the flux of >20 kev electrons drops. This shows that the dropouts of energetic electrons and protons are not associated with the entry of the satellite into a region populated by very large fluxes of 1-kev electrons or protons.

Ground magnetograms from the auroral zone are disturbed during the interval (Kp = 5+, AE = 649γ). Sudden enhancements in substorm activity are seen at about 03:15 UT near local midnight. The event is largest at Byrd (21:15 geomagnetic local time), Halley Bay (00:30), Novolazarevskaya (02:30), and Leirvogur (03:30), with an amplitude of about 800 γ. The event is seen with a smaller

amplitude and a slower onset at Baker Lake (20:00) and Lerwick (04:45). No detailed structure corresponding to the series of three dropouts in Figure 1 is evident in any ground magnetogram. The sudden expansion of the bay is very abrupt at Byrd (Figure 2), and begins at 03:14. The declination record shows several small oscillations beginning 7 to 8 minutes before the sudden expansion.

A rapid-run magnetogram is available at Leirvogur, which is at nearly the same geomagnetic local time as the satellite (Table 1). The sudden expansion begins at 03:23 to 03:24 at Leirvogur, but the activity is so intense that the magnetogram becomes illegible at 03:24. This is the same time that the newly accelerated electrons arrive at the satellite, and suggests that ionospheric currents intensify only after these particles arrive.

Figure 3 shows field and particle data for the December 1 event. Large and highly variable electron fluxes are seen for about one minute at 13:21. No protons are observed during this electron spike. The energy spectrum changes at 13:29 when the electron and proton fluxes rise suddenly. Different energy spectra have been used to normalize electron data before and after 13:29. The fluxes vary so rapidly during the 13:21 spike that it is not possible to obtain any information regarding the energy spectrum at this time. Energetic particle fluxes

fluctuated markedly until about 13:40.

The magnetometer data are quite noisy during the December 1 event. Nevertheless, the principal field changes can be seen in Figure 3. The large change in proton and electron fluxes at 13:30 is again associated with a large increase in declination. As on October 27, the equatorial portions of field lines appear to move around the earth from the tail toward the day side. No significant change in field inclination or magnitude accompanies this event.

Auroral zone magnetograms were so disturbed during this period (Kp = 8-, AE = 1351γ) that only very large field changes could be clearly identified. Sudden 1000-gamma enhancements in substorm activity were evident at about 13:30 U.T. at College (02:15 geomagnetic local time) and Baker Lake (06:15). College is at nearly the same geomagnetic local time as the satellite. The horizontal trace of the storm magnetogram is shown in Konradi's (1968) Figure 4. The rapid-run magnetogram shows the sudden enhancement in activity beginning at 13:29. The activity is so intense that the magnetogram becomes illegible at 13:30. The electrons that are seen after 13:29 may have been accelerated during the substorm.

Sudden commencement event. Figure 4 shows data from the October 28 event. The satellite was nearer to the

equator and at a higher altitude during this event than during the other two events (Table 1). A storm sudden commencement was reported at 50 ground stations at 08:10 (Lincoln, 1962). No substorm activity is associated with the sudden commencement. Konradi (1968) concluded that the flux changes seen during this event could be produced by an adiabatic compression of the magnetosphere.

The magnetic field changes between 08:09 and 08:12 in Figure 4 are just what would be expected if the viscous drag and the total pressure exerted by the solar wind were to increase. The increased drag would produce a negative change in declination as field lines are pulled back into the tail more rapidly. The pressure increase would increase the field magnitude and inclination angle as the entire magnetosphere is compressed.

The field magnitude shows a single compressional pulse at 08:13, and then becomes stable at a level that is 25 gammas higher than the level seen before the sudden commencement. Oscillations with a period of 240 seconds are seen in the declination angle. They are damped with a characteristic period of about 500 seconds until 08:24, when they disappear. These observations provide evidence that the equatorial part of field lines can sustain torsional oscillations.

Ground magnetograms from most auroral stations show

a single pulse in the H-component of the field. The field rises by about 50 gammas in one or two minutes and then returns to its original level. No such pulse is seen at most equatorial stations, but there is a sudden permanent 30-gamma increase in field strength. We could not find the 240-second declination oscillations in any ground magnetogram. These correlations suggest that the satellite magnetometer detected at least three separate waves that were excited during the sudden commencement; a single pulse propagating roughly along field lines to the auroral zone, a compressional wave propagating roughly perpendicular to field lines to equatorial ground stations, and a torsional oscillation that is largely confined to the outer magnetosphere.

The increased flow of field lines into the tail may be important in initiating the onset of some substorms that accompany SSC's. During this SSC, however, the only observed effects of the increased viscous drag were changes in the magnetic field declination.

Detailed particle-field correlations. Both energetic particle and magnetic field measurements were made three times per second. This provided about six measurements during each 2-second satellite spin period. The ion-and-electron detector looks at an angle of 45° with respect to the satellite spin axis, so that a 90° full-width cone

is scanned. When we look at individual data points, it is possible to study the rapid flux changes and to estimate flux gradients, plasma flow speeds, and the resulting electric fields.

Figures 5a and 5b show typical fluxes measured by the ion-and-electron detector within the magnetosphere. The detector samples a given pitch angle twice during each spin period and 4 or 5 times during each 5-second interval when fluxes in a fixed energy band are being sampled. The flux at a given pitch angle usually remains constant while the 4 or 5 measurements are made (Figures 5a and 5b).

If a very steep flux gradient exists, the fluxes measured at a fixed pitch angle, but at different azimuthal angles around the field line, will differ. A measurement of this east-west, or azimuthal asymmetry allows us to calculate the energetic proton flux gradient. We are, in effect, using the finite cyclotron radii of the protons to monitor events that are taking place hundreds of kilometers away from the satellite. When a steep flux gradient is present, measurements of the azimuthal distributions of particles with appropriate cyclotron radii can therefore provide nearly the same information that would be obtained with a multiple satellite experiment.

Only a limited range of azimuths were sampled because only a 90° cone is scanned. The azimuths scanned were

divided into two equal sectors, A and B. Figure 6 shows cyclotron orbits of protons entering the detector when it is looking into the two sectors. On October 27, for example, the detector is looking roughly away from the earth during one portion of the spin period. At this time, proton A will be seen. The guiding center of proton A is 34 km farther from the earth and 67 km eastward of the satellite. Later during the spin period, the detector again looks at particles with the same pitch angle as proton A, but it is now looking roughly away from the sun. At this time, proton B will be seen. This proton's guiding center is 72 km farther from the earth and 22 km westward of the satellite.

Figure 5c shows a set of proton flux measurements made on October 27 when a steep gradient existed. Even though the flux was decreasing slowly during the 5-second interval shown, it is clear that the flux was higher at any pitch angle in sector A than it was at the same pitch angle in sector B. The average proton entering sector A has a guiding center that is closer to the earth and also closer to the sun than the guiding center of the average proton entering sector B. The observed asymmetry, therefore, could be produced by a flux that increases as one moves toward the earth or by a flux that increases as one moves eastward, toward the sun. All significant flux

asymmetries we have found yield gradients pointing in this same direction.

Figure 5d shows the electron fluxes that were measured during the same 5-second interval shown in Figure 5c. The first nine electron measurements made during this interval followed the typical behavior shown in Figure 5b. The tenth, eleventh, and twelvth points are 4 to 5 times below the level of the first nine points. The last three points show further fluctuations. Similar rapid fluctuations are seen frequently in electron data. Examples of much larger electron fluctuations are shown later. We have not seen any consistent azimuthal asymmetries in the electron fluxes for two reasons. First, an observable asymmetry requires a large change in the flux over one cyclotron radius. The cyclotron radii of the 20-to 100-kev electrons that we observe are about 100 times smaller than the cyclotron radii of 100-kev protons. In addition, electron fluxes often change substantially within the 1/3 second between measurements. We cannot measure an asymmetry unless the flux remains fairly constant for at least one satellite spin period.

Figures 7d, 7f, and 7g show more examples of proton asymmetries. Simultaneous electron fluxes are shown in Figures 7e and 7h (the electron flux was steady during the interval shown in Figure 7f). The occurrence of such asymmetries for a full 5-second period is relatively rare.

Usually, no significant asymmetry can be seen in either the proton or the electron flux even 10 seconds before or after the steep flux changes.

Figure 5g shows a very rapid change in the proton flux. Some asymmetry may be present during the first second of observation (first 3 data points), but it is not possible to separate an asymmetry from a time change during such a short period. The largest proton flux changes seen here are a factor of 10 drop in 1/3 second (which is probably partly produced by an asymmetry) and a factor of 100 drop in a full spin period of 2 seconds.

Figure 5h shows electron data for the same time period shown in Figure 5g. The electron flux drops by a factor of 30 within 1/3 second at a time 2/3 second after the proton flux drops. The high electron flux began to re-appear during the last 2/3 second, but the proton fluxes did not show any recovery during the 5-second interval shown in Figures 5g and 5h.

Figures 5f and 5i show two other examples of very rapid electron flux changes during the October 27 dropouts. Figures 7a, 7b, and 7c show examples of similar changes during the 13:21 electron spike on December 1, and Figure 7i shows an example of the rapid electron flux changes that are seen between 13:29 and 13:40 on December 1.

Individual magnetometer data points (3 per second) were also plotted to look at the rapid angle changes and at

the source of noise in the data. Data digitization should produce a standard deviation of 2° to 4° in the 5-second averaged inclination and declination angles plotted in Figure 4. This is close to the observed standard deviation, and we conclude that data digitization was the principal source of noise on October 28.

The magnetic field was much stronger on October 27 and December 1, so the angular errors produced by digitization are much smaller. Standard deviations of 1/4° to 1/2° would be expected in Figures 1 and 3 if the magnetic field was actually steady, and much larger standard deviations are observed. The plots of individual magnetic field data points show something about the nature of these real magnetic field fluctuations. On October 27 a number of non-periodic, saw-tooth shaped perturbations were seen in the declination angle. The overall shape of these perturbations is similar to the declination changes shown in Figures 1 except that the repetition rate is much higher and the direction of the sudden angle changes is reversed. The declination angle decreases by about 10 degrees in less than 1 second, and sometimes in less than 1/3 second. The declination angle then relaxes (increases) in 5 to 10 seconds. The "sudden" declination increases seen in Figure 1 during each dropout event appear to be extensions of the "slower" 5-to 10-second relaxations seen in the detailed plots. No increases in the declination angle on a time scale of 1 second or less

have been observed. We have not analyzed the rapid field fluctuations to see if they correspond to any simple wave mode. We also do not presently know whether such fluctuations are common or unusual. We hope to study these more carefully for a future report.

The telemetry signal was very bad on December 1, and the inclusion of bad data points produced much of the noise in Figure 3. About 30% of all individual data points were discarded by an editing routine during data processing. Nevertheless, plots of individual data points show at least some saw-tooth-shaped field fluctuations similar to those seen on October 27.

To summarize, electron fluxes frequently change abruptly within our 1/3 second resolving time. Protons require about 1 to 10 seconds to change from one stable flux level to another. When viewed on a time scale of about 5 seconds or longer, electron and proton flux changes are quite similar. The magnetic field declination changes are well correlated with particle flux changes. The declination angle increases take place in about 5 to 10 seconds. A number of more rapid (< 1 second) decreases in the declination angle are also seen during most of the time intervals shown in Figures 1 and 3, but these are not directly correlated with flux changes.

Flux gradients. The azimuthal asymmetries occasionally noted in proton fluxes provide a means of determining

the proton flux gradient. On October 27, the average proton entering the detector from sector A has a guiding center that is 89 km farther east, 96 km closer to the sun, and 38 km closer to the earth than the guiding center of the average proton entering sector B. The corresponding distances for the December 1 event are 100 km, 100 km, and 50 km, respectively (Figure 6).

We usually cannot see any significant gradient in proton fluxes. To be significant, the fluxes in sectors A and B must differ by at least a factor of 2. A characteristic distance, D, in any arbitrary x-direction over which the proton flux, ϕ, changes by a factor of e, is defined by

$$\phi = \phi_o \exp(-x/D).$$

The parameters D and ϕ_o can be evaluated from ϕ_A and ϕ_B, the fluxes measured in sectors A and B. This gives

$$D = \Delta x / \ell n(\phi_A/\phi_B)$$

as the distance one must travel in the x-direction before the flux changes by a factor of e. In the above expression, Δx is the separation, in the x-direction, between guiding centers of protons in sectors A and B. Using the separation distances quoted above and the fact that no significant asymmetries are usually seen , we conclude that the e-folding length for 100-kev proton fluxes is usually greater than 250 km in a direction parallel to the earth-sun line and is usually greater than 100 km in the radial direction.

We occasionally (Figures 5c, 7d, 7f, 7g) see significant proton flux asymmetries, which imply that the gradient is steeper than the above limits. There are six 5-second periods on these two days when proton fluxes in the two sectors differed by factors of 2 to 4. If the gradient is assumed to be parallel to the earth-sun line, the e-folding length must be about 90 km. If the gradient is directed radially toward the earth, the e-folding length must be about 40 km. It is not possible to pick any direction for the proton gradient that results in an e-folding length that is greater than 100 km during these brief intervals. These lengths may be compared to the cyclotron radius of a 100-kev proton, which is about 75 km to 100 km in these regions.

We can draw one important conclusion from the fact that steep flux gradients occasionally exist: The boundary that passes the satellite is much thinner than the ordinary high-latitude trapping boundary. We have never detected any measurable gradient in the ordinary high-latitude boundary over the night side of the earth.

The observed gradients are also much too steep to be maintained as protons and electrons drift around the earth. Even if there was no scattering of energetic particles, shell-splitting effects would broaden an initially steep gradient as particles drift around the earth. Particles that start at noon on a given field line, but with various pitch angles, are spread over a band of field lines when

they drift to midnight. Roederer's (1967) calculations show that this radial spreading is about 2000 km on the L = 5 field line as seen by a satellite at the equator, and about 400 km as seen by a satellite at a 30° latitude. This is a factor of 10 thicker than the measured radial gradients.

The near coincidence of 20-kev electron and 100-kev proton gradients also suggests that the particles have not drifted very far around the earth. These energetic particles do not have identical drift paths in the presence of electric fields, and neither group will follow the drift motion of the bulk of low energy particles that maintain approximate charge neutrality.

We conclude that the observed flux gradient does not originate over the day side of the earth and then drift to the detectors. It must be produced locally, near the satellite. The plasma beyond the trapping boundary is therefore probably incapable of sustaining large fluxes of energetic trapped particles.

DISCUSSION

The observations made during the substorm-associated events allow us to draw several conclusions regarding field-line motion, plasma flow, electric fields, and the acceleration of energetic particles.

Temporal and spatial character of flux changes. We agree with Yeager and Frank's (1969) conclusion that the observed flux changes must be produced by the motion of a relatively steady flux gradient past the satellite. The alternatives are: to accelerate and decelerate or precipitate energetic particles very rapidly, or to suddenly break and reconnect field lines. The breaking of a field line could produce a sudden decrease in energetic particle fluxes because a trapping geometry would suddenly cease to exist. It is also conceivable that some other disturbance could cause energetic particles to be precipitated rapidly, though we know of no mechanism that can change fluxes by two to three orders of magnitude in less than two seconds. By comparison, the bounce periods for 20-kev electrons and 100-kev protons are 3 seconds and 30 seconds. If the flux is to drop by a factor of 100 in less than a bounce period, particles would have to interact with a nearly perfect absorber. The ionosphere, for example, would scatter back more than 1% of an incident beam of electrons. Scattering in the tail would also be expected to return some of the particles

moving out an open field line. Finally, it is doubtful whether a field line as low as L = 5 can open and reconnect.

The sudden electron (Figure 5f) and proton (Figure 7d) flux increases are even more difficult to explain without proposing that a flux gradient moves past the satellite. If energetic particles are lost from field lines, the field lines will become repopulated as new particles drift onto them. The fluxes are observed to recover to nearly the same levels seen before the dropouts in less than one-bounce period. The pitch angle distributions of the first particles observed also appear to be normal. Finally, electron and proton fluxes both change together when viewed on a 5-second time scale. We know of no way that drifting particles can repopulate field lines in this manner. We conclude that we are observing the effects of the rapid bulk motion, past the satellite, of plasma containing a steep, relatively steady energetic particle flux gradient.

Speed of field line motion. Figures 5g and 7d show that proton fluxes change by a factor of 100 or more within one spin period (2 seconds). Assuming that an exponential flux profile is being swept past the satellite at a speed v, the ratio of fluxes seen at times t_2 and t_1 is

$$\phi_2/\phi_1 = \exp\ [v(t_1-t_2)/D]$$

where D is the e-folding length defined previously. The velocity required to produce a 100-fold flux change in 2 seconds is 90 km/sec if the flux gradient moves radially

toward or away from the earth (D = 40 km) and 200 km/sec if the motion is around the earth in longitude, i.e., roughly toward or away from the sun (D = 90 km). Even larger velocities would be required to produce the 10-fold flux changes in 1/3 second shown in Figures 5g and 7d. These 10-fold changes are, however, produced partly by the flux asymmetry. Fluxes in sector A are about 3 times as high as the fluxes in sector B at the same pitch angle during these intervals, so the motion of field lines need produce only an additional 3-fold change in 1/3 second. This change implies velocities only slightly higher than those quoted above.

The alternative to concluding that the plasma flows at a speed of at least 100 km/sec is to conclude that the e-folding lengths are much shorter than the above estimates. It is not possible to measure the e-folding lengths during the most rapid flux changes, so we have assumed that they are the same as the shortest e-folding lengths that we have been able to measure. This assumption is supported by the following observations. The asymmetry can be measured immediately after the steepest rise in Figure 7d, and is nearly the same as the asymmetry seen during other dropouts (the flux in sector A is 3 times the flux in sector B). The first three points in Figure 5g also provide evidence for an asymmetry of about the same magnitude. The asymmetry can be measured during most of the rapid flux change in Figure 7g, and is again nearly the same magnitude. This

last flux change requires a velocity of 50 km/sec radially or 100 km/sec toward the sun. Asymmetries can be measured throughout slower flux changes (Figures 5c and 7f). These data require velocities of only 10 km/sec radially or 20 km/sec toward the sun.

If the factor of 100 flux changes in 2 seconds were to be produced by a plasma moving at only 10 km/sec, then a 4-km e-folding length would be required. This may be compared to the 75 km to 100 km cyclotron radii of 100-kev protons. We know of no theoretical reason that would prohibit such steep gradients, but we also know of no mechanism that could produce 100-kev proton flux gradients of this magnitude in this region of the magnetosphere. A plasma discontinuity that is thinner than 4 km could certainly be present. The observed protons could also be scattered either at the discontinuity or in the plasma on one side. These scattered protons would then be lost into the atmosphere. It is conceivable that if such a discontinuity was stationary for many proton bounce periods and if the discontinuity accurately followed a proton drift path, then a very steep proton gradient could be set up. The observed complex sequence of rapdi flux changes, however, shows that conditions change substantially during a single proton bounce period. We also see no reason to believe that a plasma discontinuity will accurately follow the drift path of a 100-kev proton. The plasma discontinuity should be aligned with the drift paths

of electrons and protons in the background plasma. The drift paths of particles with energies near or below 1 kev are strongly influenced by any electric field that can produce even a 10 km/sec bulk plasma flow. The 100-kev protons, however, are not strongly influenced by this electric field, so their drift paths are determined almost entirely by the magnetic field gradient and curvature.

It is interesting to compare the observed asymmetries with those seen at the magnetopause. The magnetopause is a plasma discontinuity that is much thinner than the gyroradius of a 100-kev proton. We have made frequent measurements of proton asymmetries at the magnetopause, and have never seen e-folding lengths much shorter than the proton cyclotron radius. In fact, the steepest gradients seen at the magnetopause produce about the same factor of 3 difference between fluxes in sectors A and B that is reported here.

We therefore conclude that the proton e-folding length does not become much shorter than the proton gyroradius. This means that the proton flux gradient must occasionally move past the satellite at a speed of at least 100 km/sec.

We can also set an approximate upper limit on the plasma flow speed. If a cold background plasma were to move at 400 km/sec, the protons would have enough flow energy to be seen by the CdS detector. If the background plasma was hot, the flux seen by the CdS detector would still increase if the plasma began to flow at 400 km/sec. For

example, the energy flux of a group of initially isotropic 1-kev protons would increase by a factor of 3 if they acquired a bulk velocity of 400 km/sec. The only changes in CdS flux that we have observed are very similar to the changes in 20-kev electron fluxes, which are not significantly influenced by a 400 km/sec bulk flow. These observations suggest that the CdS detector is not responding to changes in the bulk flow velocity, and therefore that plasma does not flow faster than about 400 km/sec.

Once the flow speed is known, it is possible to estimate an upper limit to the electron e-folding length. It was previously noted that electron fluxes change by large factors in less than one second, while proton fluxes require several seconds to make similar changes. This suggests that 20-kev electron gradients are at least 10 times steeper than 100-kev proton gradients. Characteristic electron e-folding lengths must therefore be less than 10 km. The cyclotron radii of these electrons are about 1/2 km to 1 km.

Finally, it is possible to estimate the average radial velocity of the trapping boundary. Crossings are made at 03:13, 03:19, and 03:24 on October 27, when the satellite is at L = 4.74, 5.02, and 5.23. The satellite was outbound with a radial speed of 3 to 4 km/sec during both substorms. We conclude that the steep flux gradient moves outward about 0.5 L shells in 11 minutes. The invariant latitude of this

trapping boundary moves poleward by 1.4°, from 62.7° to 64.1° during this period. This corresponds to a poleward motion at about 0.2 km/sec in the auroral ionosphere. On December 1, the trapping boundary overtakes the satellite at 13:29, and is not seen again. It therefore must have moved outward at least as fast as the above estimates for October 27.

Temporal and spatial character of magnetic field changes. It is difficult to separate temporal from spatial aspects of the magnetic field changes because we cannot measure magnetic field gradients. The observed perturbations appear to be neither purely temporal nor purely spatial.

The simplest model involves a steady, frozen-in magnetic field structure that moves back and forth past the satellite along with the steady particle gradient. The 03:13 dropout on October 27 is the only event that fits this model even moderately well. The declination angle suddenly increases when the particle fluxes drop out, and suddenly decreases when particle fluxes return. Even in this case, the magnetic field does not fully return to the original direction after the dropout. This shows that at least part of the magnetic field variation must be temporal. The 03:19 dropout also shows that the magnetic field structure is not steady. At 03:19, the declination increase is much steeper than the decrease, even though the particle

flux increase and decrease have roughly comparable time scales.

On December 1, we see no significant field change during the 13:21 electron spike. Only a moderate field change accompanies the flux increase at 13:29. Most of the declination change associated with this event takes place one minute later, and is not accompanied by any significant particle flux change.

These observations suggest that a current sheet is flowing very near the outer boundary of trapped particles, but that the current sheet is not steady. Changes in the current flow would be expected to accompany changes in the plasma flow speed, and changes in the associated electric field.

The lack of a current sheet at 13:21 on December 1 suggests the absence of rapid plasma flow at this time. It is quite likely that the 13:21 electron spike was not directly associated with the 13:29 substorm event, but with other intense activity that began at 12:52 and at 13:05 (Lincoln, 1962). A steep flux gradient persisted for at least 11 minutes on October 27, and so could have persisted until 13:21 on December 1. The fact that only electrons were seen at 13:21 suggests that energetic electron and proton gradients may have separated slightly by this time.

The large angle change just after 13:30 on December 1 could be produced by the passage of the satellite through

a current sheet that is located inside the trapped particle region. Alternatively, this angle change could be purely temporal. In the latter case, the current sheet would be coincident with the trapping boundary, and would simply intensify about one minute after the satellite crossed this boundary. There does appear to be a small increase in declination at 12:29 (Figure 3), corresponding to a current sheet on the trapping boundary.

On October 27, all the sudden magnetic field declination changes are coincident with crossings of a flux boundary. Whenever a thin current sheet exists on this day, it seems to be located very near the flux boundary. The strength of the current sheet is different during each crossing, and a thin sheet may even be absent when the 03:19 flux recovery is seen.

Plasma flow. It is not possible for the gradient to be consistently moving radially toward or away from the earth at 100 km/sec on October 27, because it is seen to remain near the satellite for at least 11 minutes. We conclude that most of the bulk plasma flow must be directed eastward or westward, around the earth.

Both the energetic particle flux changes and the plasma flow character look quite similar to data seen when the satellite makes multiple crossings of the magnetopause. Figure 8a shows a sketch of a model that is consistent with our observations. Waves are shown near the high latitude

trapping boundary, and these waves are blown around the earth by the rapid plasma flow, just as waves on the magnetopause appear to be blown into the tail by the solar wind (Kaufmann and Konradi, 1969a; Aubry, et al., 1971). The motion of waves produces rapid local motions of the boundary toward and away from the earth. The waves may be produced by the Kelvin-Helmholtz instability, but we have been unable to test this suggestion. The criteria for onset of this instability depend sensitively upon the change in the direction of the magnetic field across the boundary (Sen, 1965; Southwood, 1968). We are unable to measure this angle change because of the difficulty in separating temporal from spatial changes in the magnetic field. We have concluded that the current sheet at the boundary varies with time, so the magnetic field direction change will also vary.

Figure 8b shows a different model of plasma motion that could produce multiple crossings of the flux gradient. This is the model proposed by Yeager and Frank (1969). In this model, plasma moves radially toward and away from the earth and field lines are stretched out and compressed. This model predicts that the inclination angle should be correlated with flux changes and that the declination angle should remain constant. We observe just the opposite effect. This model is also not consistent with a 100 km/sec flow speed because flow in this model is not restricted to a narrow band. It is shown in the section on electric fields that

unacceptably large potential drops are required to drive the whole plasmasphere in any oscillation that involves 100 km/sec flow speeds.

Current flow. Our observations do not provide very strong support for the model current systems that are commonly used in auroral theories. We are severely limited in deriving a current system because we have data from only two substorms, and because there are important differences in the magnetic field distortions seen during these two events.

The most important difference between the two events is that the field moves toward the sun on October 27 each time the satellite leaves the stable trapped particle region, and toward the sun at 13:30 on December 1 when the satellite enters a not-so-stable trapped particle region.

Sunward bending of field lines can be produced by three field-aligned sheet-current systems. If a single sheet current flows down field lines to the ionosphere, we should see the observed sunward distortion when the satellite is below the current sheet. If a single current sheet flows away from the earth, field lines above the sheet will be moved toward the sun and those below the sheet will move toward the tail. With a double current sheet, field lines between the two current sheets will move toward the sun if current flows down at high latitudes (e.g. upward flow of electrons) and up at low latitudes (e.g. electron precipitation). Armstrong and Zmuda (1970) and Choy, et al., (1971)

have presented evidence to support the presence of currents flowing in this direction.

Figure 8c shows a slightly modified version of a single-current-sheet model (see Alcasofu, 1968) that produces field changes in the direction seen by the satellite on December 1. To explain the observations, the downward current must flow in a sheet at dawn, and the satellite observes a sunward distortion as the sheet moves radially outward to overtake the satellite. This model must be further modified as in Figure 8d if it is to explain the October 27 data also. Here the downward current flow is unchanged, but the upward current flow forms a sheet that extends over the entire night side of the earth. The satellite must cross the upward current flow region on October 27 to see the field distorted more toward the sun beyond the trapping boundary. Both these systems are completed by a portion of the auroral electrojet current in the ionosphere. A portion of the auroral electrojet may also be closed by currents that flow entirely within the ionosphere. At high altitudes the field-aligned currents are closed by partial ring currents, by current flow across the tail, or by flow directly from the solar wind via the dayside cusps. One important drawback of both models is that they predict a net tailward displacement of field lines on one side of the current sheet, while we observe only varying degrees of sunward distrotions relative to the orientation seen before the substorm. This

distortion fits more naturally into a double-current-sheet model. An even more serious drawback involves the electric field structure. In the next section it is shown that the intense electric fields that are required to produce the rapid plasma flow must be limited to a thin region, such as the region between two current sheets.

The model in Figure 8e fits the October 27 data very well. Field lines are distorted toward the sun between the current sheets, and are not strongly distorted elsewhere. The upward current sheet is roughly coincident with the high-latitude trapping boundary, so field lines are distorted toward the sun when the satellite enters the low-flux region. It is possible that the satellite crosses the downward current sheet just before 03:25. At this time, the declination angle decreases and particle fluxes show a secondary decrease. If this had been another crossing of the upward current sheet seen earlier, energetic particle fluxes would have increased to their original levels when the declination angle decreased.

The December 1 data agrees reasonably well with Figure 8e except that in this case the downward current sheet must be closer to the high-latitude trapping boundary. An upward current sheet may be crossed at 13:40 when fluxes become stable. It is not surprising that significant variations are seen between the locations of current sheets and the trapping boundary. The current sheet is not

directly related to the 20-kev electrons or 100-kev protons that we observe. It is probably at either the plasmapause or at the inner edge of the plasma sheet. Frank (1971) has shown that there are considerable variations between the locations of these three boundaries. On October 27 the steep flux gradient is apparently nearly coincident with the plasmapause or with the edge of the plasma sheet.

Electric fields. The high plasma flow velocities require the presence of large electric fields in the satellite's (or the earth's) reference frame, assuming that the electric field is small in a reference frame moving with the plasma. The electric field component directed perpendicular to the magnetic field direction is given by

$$E_{\perp} = Bv_{\perp}/c$$

in Gaussian units, where $v_{\perp}$ is the plasma flow speed perpendicular to B. When the highest flow velocities are observed on October 27 and December 1, $B \doteq 790$ gammas and $B = 560$ gammas, respectively. These figures show that electric fields as high as 50 to 100 mV/m must occasionally exist at 30° geomagnetic latitude on the $L = 5$ field line.

It is clear that 50 to 100 mV/m fields cannot extend over a large region of the magnetosphere. If the flow region is 500 km thick, the total potential drop required across the region is 25 to 50 kV. If the flow region is one earth radius thick, then the potential drop must be 300 kV to 600 kV. A total potential drop of 3 to 6 MV would be

required to move the entire plasmasphere at 100 km/sec. We conclude that the rapid plasma flow must be restricted to a narrow band or channel within the magnetosphere.

The electric fields and flow velocities that would be seen near the equator and near the earth can be calculated if the magnetic field lines are assumed to be equipotentials. The magnetic flux contained between two shells of field lines that intersect the earth at invariant latitudes Λ_1 and Λ_2 is given by

$$\Phi = \Delta\phi \; \ell \; B \; R \cos \lambda$$

where $\Delta\phi$ is the angular extent of the shells in longitude, and ℓ is the distance between the shells at a radial distance, R, and at a latitude, λ. The magnetic flux between these shells is constant, and the electric field is inversely proportional to ℓ if the field lines are equipotentials, so $(R \; B \cos \lambda)/E$ = constant. Assuming that field lines at L = 5 are nearly dipolar, $R \doteq L \cos^2\lambda$. The electric field and plasma drift velocity therefore vary as $B \; L \cos^3\lambda$ and $L \cos^3\lambda$, respectively.

As an example, we will assume that plasma flows at 100 km/sec in a region 500 km thick at the satellite location ($\lambda = 30°$ on the L = 5 field line). This implies a local electric field of 70 mV/m, and a total potential drop of 35 kV across the flow region. At the equator, the electric field would be 35 mV/m; the flow velocity, 150 km/sec; and the flow region, 1000 km wide. Near the earth, in auroral

regions, the electric field would be 750 mV/m; the flow velocity, 13 km/sec; and the flow region 45 km wide.

Some mechanism probably reduces the conductivity along field lines so that the large electric fields do not penetrate deeply into the ionosphere. Carlqvist and Boström (1970) suggested that space-charge regions could produce the required high impedance. Alfvén and Carlqvist (1967) described how this mechanism can produce very high electric fields that are confined to a narrow band. The high fields are produced when current flow in the ionosphere exceeds a critical maximum level that can be carried. Kindel and Kennel (1971) proposed a wave-instability mechanism that can also reduce the conductivity along field lines if the field-aligned currents exceed a critical value.

The observed field distortions require the presence of 100γ to 200γ perturbation magnetic fields. These fields can be produced by a 1×10^{-3} amp/cm sheet current density near the satellite. If this current flows down to ionospheric levels, it will be doubled by geometrical factors. Both conductivity-lowering mechanisms described previously require volume current densities that exceed a critical value, and we have no direct measurement of a volume current density. We can make an unsupported guess that the current flows in a sheet that is 10 km thick at ionospheric levels. With this guess, the volume current density becomes 2×10^{-9} amp/cm^2 at ionospheric levels. This could be produced

by a flux of 1×10^{10} electrons/$cm^2 \cdot$ sec at the ionosphere. These estimates are near the limiting current densities required by both conductivity-lowering mechanisms.

We can compare the fields we measure with electric fields that have been measured by other methods. Carpenter (1970) has reviewed the electric fields deduced from whistler observations. Near local midnight, peak equatorial fields of 0.5 to 2 mV/m are inferred from tracking the cross-L drift of whistler ducts, primarily within the plasmasphere. Peak fields about twice this large are inferred within the dusk side plasmasphere from motion of the bulge.

It is not surprising that we measure significantly different electric fields from those deduced from whistler duct measurements. The field distortion suggests that we are observing motion that is directed around the earth in longitude. Whistlers change properties only when the ducts move across L-shells. The trans-L drift of whistler ducts is more directly related to the 3 to 4 km/sec net radial velocity of the trapping boundary. This velocity requires an electric field of slightly over 1 mV/m at the equator, in good agreement with whistler observations.

Flow velocities of 30 km/sec have been reported near the equator by Freeman (1968). These observations were associated with intense magnetic storms, so may be related to the events discussed here. The highest plasma speeds that we measured were seen on lower field lines than those

sampled by the ATS satellite.

Hallinan and Davis (1970) have reported motions in auroral arcs that imply the presence of 500 mV/m to 1000 mV/m electric fields near the earth. The events we see may be related to auroral arcs, but this relationship is quite uncertain. We have only seen steep flux gradients during two very intense substorms, while auroral arcs are frequently present.

Hones, et al. (1971) have observed several hundred km/sec plasma flow speeds at 18 Re in the magnetotail plasma sheet during substorms. This flow is not directed toward the sun, but has a sunward component. It is possible that the rapid flow region extends from the trapping boundary all the way to 18 Re and beyond, but we have no way to check this possibility at present.

The direction of the electric field must be either toward the earth (equatorward in the ionosphere) or away from the earth (poleward in the ionosphere) so that the E X B drift of plasma will be around the earth in longitude. The equatorward field is needed if we are to close a two-sheet current system in the ionosphere by a Pedersen current. The Hall current from a westward electric field could also close the current system in the ionosphere. The presence of a westward electric field would, however, produce an inward drift of the flux gradient, and a net outward drift is observed. It appears that the current system is completed

in the ionosphere by the Pedersen current from an equatorward electric field. The resulting E X B drift of plasma is around the earth from the tail toward the day side.

Figure 8e shows the two-sheet current system closing near the equator by currents flowing across field lines. In the MHD approximation, the current that flows perpendicular to a magnetic field is given by

$$J_{\perp} = \frac{c}{B^2} \underset{\sim}{B} \times \left(\rho \frac{\partial \underset{\sim}{v}}{\partial t} + \rho \, (\underset{\sim}{v} \cdot \nabla) \underset{\sim}{v} + \nabla p \right)$$

The first two terms could be associated with significant fluctuating currents in the presence of waves similar to that shown in Figure 8a. It is, however, highly unlikely that they are associated with the relatively steady current system shown in Figure 8e, and certain that they are not associated with the steady currents described by Armstrong and Zmuda (1970). A current density of 6×10^{-13} amp/cm^2 must flow across dipole field lines from the satellite to the equator in order to produce the estimated 1×10^{-3} amp/cm sheet current at the satellite. If there are 10 particles/cm^3, the velocity would be required to uniformly decrease by 100 km/sec every 2 seconds if the first term is to balance the force produced by $J_{\perp}$. With the same density estimate, the flow velocity would have to uniformly decrease by 100 km/sec every 200 km that an observer moves in longitude toward the tail for the second term to be dominant. The above characteristic time and length are both proportional

to the particle number density, so are not likely to be important unless the number density exceeds 10^3 particles/cm^3.

The pressure gradient term is a more likely source of currents near the equator. In the dawn hemisphere, a current in the direction shown will be produced by a westward pressure gradient (plasma pressure increasing toward the tail). A fairly large gradient is required to complete the circuit when 100 km/sec flow is seen. Assuming that the outward current flow is uniform near the equator, and that the average electron and proton energies are 2 kev, then the number density of electrons and protons must change by 10 particles/cm^3 per earth radius as one moves in longitude. The required number density gradient is smaller if the particles have a larger average kinetic energy. If currents from a particle pressure gradient that points toward the tail is responsible for closing the current system, then currents on the dusk side of the earth would flow in the opposite direction (i.e. toward the earth at the equator).

Finally, it is possible that the L = 5 field line does not have the roughly dipole shape shown in Figure 8e. If this field line is stretched well out into the tail, then currents could close in a region containing a very weak magnetic field. As an example, assume that the L = 5 field line is distorted so that it passes 2 earth radii into a region containing a 10γ magnetic field. Then the pressure

gradient term can account for the required current flow if the density of a 2-kev plasma increases by 1 particle/cm^3 for each earth radius an observer moves westward from the dawn boundary of the tail. A reverse current flow is again required wherever the gradient reverses direction.

Particle acceleration. The presence of large electric fields can produce rapid adiabatic and non-adiabatic changes in the energies of electrons and protons. Particles that move in from the tail with the convection system are heated adiabatically. At 100 km/sec, they can move several earth radii in several minutes. This rapid convection could be especially important in the acceleration of Mev particles in the outer zone (Kaufmann and Konradi, 1969b).

Particles that either drift or are scattered out of the convection system behave non-adiabatically. The total potential difference across the cyclotron orbit of a 100-kev proton is more than 10 kV in the rapid flow region. Only a few scattering events are therefore needed to significantly change the energy of such a proton.

Energetic particles that drift out of a convection system can gain either more or less energy than the lower energy particles that remain in. Line curvature and magnetic field gradient drifts can carry energetic particles across the potential drop that produces convection. To be efficient, the drift speed should be comparable to the plasma flow speed. Drift speeds of 20-kev and 100-kev

particles at L = 5 are about 1 km/sec and 10 km/sec, respectively, so non-adiabatic effects should be seen primarily in 0.1 to 1 Mev particle fluxes. Drift effects are not expected to produce large non-adiabatic energy changes near the satellite on October 27 or December 1 because the direction of the drift velocity is nearly parallel to the plasma flow direction at these locations. Hones, et al. (1971) have observed rapid flow at 18 Re in the plasma sheet. If this rapid flow extends all the way to 5 Re, drift effects should produce important non-adiabatic energy changes. These drift effects may be important in explaining the observed sudden changes in 0.1 to 1 Mev proton (Konradi, 1967; Fennell, 1970) and electron (Hones, et al., 1970) fluxes.

Table 1

Day	U.T.	GM Lat.	GM Local Time	L(Re)	R(Re)	$B_{JC}(\gamma)$
Oct. 27	03:10	-29	03:27	4.7	3.5	922
Oct. 27	03:30	-28	04:04	5.5	4.1	547
Oct. 28	08:00	-13	06:06	7.9	7.4	79
Oct. 28	08:30	-11	06:20	8.5	8.1	61
Dec. 1	13:20	-31	02:44	5.4	3.9	735
Dec. 1	13:50	-28	03:19	6.3	4.9	355

ACKNOWLEDGMENTS

We wish to thank L. J. Cahill, Jr. for the use of Explorer 12 magnetometer data and L. R. Davis for the use of ion-and-electron detector data. The CdS detector data was supplied by the National Space Science Data Center.

This work was supported in part by the Atmospheric Sciences Section, NSF grant GA-14954.

REFERENCES

Akasofu, S.-I., Polar and magnetospheric substorms, D. Reidel Publishing Company, 1968.

Alfvén, H., and P. Carlqvist, Currents in the solar atmosphere and a theory of solar flares, Solar Phys., 1, 221, 1967.

Armstrong, I. C., and A. I. Zmuda, Field-aligned current at 1100 km in the auroral region measured by satellite, J. Geophys. Res., 75, 7122, 1970.

Aubry, M. P., M. G. Kivelson, and C. T. Russell, Motion and structure of the magnetopause, J. Geophys. Res., 76, 1673, 1971.

Brown, W. L., L. J. Cahill, L. R. Davis, C. E. McIlwain, and C. S. Roberts, Acceleration of trapped particles during a magnetic storm on April 18, 1965, J. Geophys. Res., 73, 153, 1968.

Cahill, L. J., and P. G. Amazeen, The boundary of the geomagnetic field, J. Geophys. Res., 68, 1835, 1963.

Carlqvist, P., and R. Boström, Space-charge regions above the aurora, J. Geophys. Res., 75, 7140, 1970.

Carpenter, D. L., Whistler evidence of the dynamic behavior of the dusk side bulge in the plasmasphere, J. Geophys. Res., 75, 3837, 1970.

Choy, L. W., R. L. Arnoldy, W. Potter, P. Kintner, and L. J. Cahill, Jr., Field aligned particle currents near an auroral arc, Univ. of N.H. Research Report, 1971.

Davis, L. R., and J. M. Williamson, Low energy trapped protons, Space Res., 3, 365, 1963.

Fairfield, D. H., Average magnetic field configuration of the outer magnetosphere, J. Geophys. Res., 73, 7329, 1968.

Farnell, J. F., Observations of proton bursts in the magnetotail with Explorer 35, J. Geophys. Res., 75, 7048, 1970.

Frank, L. A., Relationship of the plasma sheet, ring current, trapping boundary, and plasmapause near the magnetic equator and local midnight, J. Geophys. Res., 76, 2265, 1971.

Freeman, J. W., Jr., The morphology of the electron distribution in the outer radiation zone and near the magnetospheric boundary as observed by Explorer 12, J. Geophys. Res., 69, 1691, 1964.

Freeman, J. W., Jr., Observation of flow of low-energy ions at synchronous altitude and implications for magnetospheric convection, J. Geophys. Res., 73, 4151, 1968.

Hallinan, T. J., and T. N. Davis, Small-scale auroral arc distortions, Planet. Space Sci., 18, 1735, 1970.

Hones, E. W., Jr., R. H. Karas, L. J. Lanzerotti, and S.-I. Akasofu, Magnetospheric substorms on September 14, 1968, Los Alamos preprint LA-DC-12253, 1970.

Hones, E. W., Jr., S.-I. Akasofu, S. J. Bame, M. D. Montgomery, and S. Singer, Magnetotail plasma flow measured with an electrostatic analyzer on Vela 4A, Trans. A.G.U., 52, 325, 1971.

Jensen, D. C., and J. C. Cain, An interim geomagnetic field (abstract), J. Geophys. Res., 67, 3568, 1962.

Kaufmann, R. L., and A. Konradi, Explorer 12 magnetopause observations: large-scale nonuniform motion, J. Geophys. Res., 74, 3609, 1969a.

Kaufmann, R. L., and A. Konradi, Mev particles in the outer zone: Explorer 12, Univ. of N.H. Research Report, UNH-R69-5, 1969b.

Kindel, J. M., and C. F. Kennel, Topside current instabilities, J. Geophys. Res., 76, 3055, 1971.

Konradi, A., Rapid increases in the proton and electron fluxes in the magnetosphere, J. Geophys. Res., 73, 3449, 1968.

Lincoln, J. V., Geomagnetic and solar data, J. Geophys. Res., 67, 2975, 1962.

McPherron, R. L., and P. J. Coleman, Jr., Magnetic fluctuations during magnetospheric substorms 1. expansion phase, J. Geophys. Res., 75, 3927, 1970.

Mead, G. D., and L. J. Cahill, Jr., Explorer 12 measurements of the distortion of the geomagnetic field by the solar wind, J. Geophys. Res., 72, 2737, 1967.

Roederer, J. G., On the adiabatic motion of energetic particles in a model magnetosphere, J. Geophys. Res., 72, 981, 1967.

Sen, A. K., Stability of the magnetospheric boundary, Planet. Space Sci., 13, 131, 1965.

Southwood, D. J., The hydromagnetic stability of the magnetospheric boundary, Planet. Space Sci., 16, 587, 1968.

Yeager, D. M., and L. A. Frank, Large temporal variations of energetic electron intensities at midlatitudes in the outer radiation zone, J. Geophys. Res., 74, 5697, 1969.

FIGURE CAPTIONS

Figure 1. The top curve shows the maximum flux of >20 kev electrons seen during each 5-second sampling interval. The middle three curves show the differences between the observed magnetic field declination, inclination, and magnitude and the values of these quantities calculated by the Jensen and Cain (1962) model. The bottom curve is the count rate of the cadmium sulfide total energy detector.

Figure 2. Tracings are shown from the Byrd normal and rapid-run magnetograms.

Figure 3. Similar to Figure 1.

Figure 4. Similar to Figure 1.

Figure 5. Count rates measured at 1/3 second intervals are shown as a function of pitch angle. The letters A and B near proton data points indicate the sector into which the detector was looking at the time of measurement. Proton counts are accumulated for 1/3 second. Each proton point therefore represents the total number of counts recorded over a range of pitch angles that extends roughly half way to the closest adjacent points. Electron fluxes are essentially instantaneous measurements at high flux levels, but the time constant becomes significant as background is approached. The electron background is at 9 on the count-rate scale, and the proton background is at 3, though proton fluxes become unreliable below a level of 10.

Figure 6. Trajectories of 100-kev protons that enter the detector are sketched in a plane normal to the magnetic field. Field lines point directly up from the plane of the figures. Dots show the guiding centers of the average protons entering the detector from sectors A and B, and arrows show the directions of the earth and sun.

Figure 7. Similar to Figure 5.

Figure 8. Panel a is a sketch of a model of field line distortion and plasma motion that is consistent with the data. Heavy lines represent the magnetopause and the high-latitude trapping boundary. Light lines represent equatorial intersections of magnetic field lines that intersect the earth at various local times. Panel b shows an alternative model for plasma motion that is not consistent with the data. Panels c, d, and e show possible current systems. In models c and d, the current system is completed by a partial ring current or by currents flowing from the tail or from the dayside cusps. Model e provides the best fit to our data.

Table 1. Satellite orbital parameters are given for times corresponding to the ends of the intervals shown in Figures 1, 3 and 4. R is the radial distance to the satellite and B_{JC} is the magnitude of the Jensen and Cain (1962) model field that has been subtracted from the measurements to form the differences shown in Figures 1, 3 and 4.

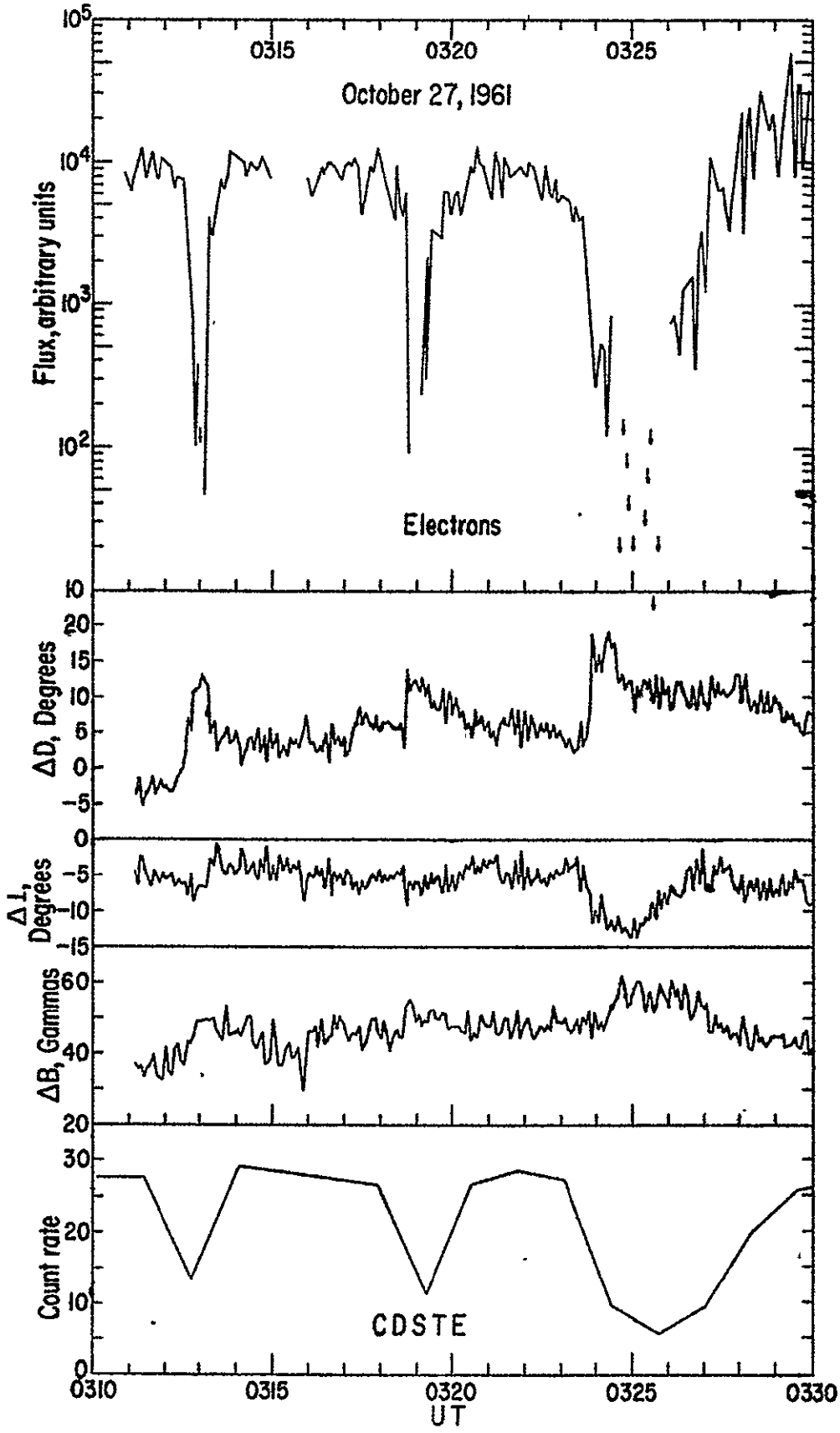
October 27, 1961
Flux, arbitrary units
Electrons
ΔD, Degrees
ΔI, Degrees
ΔB, Gammas
Count rate
CDSTE
UT
0315
0320
0325
0310
0330

Figure 1

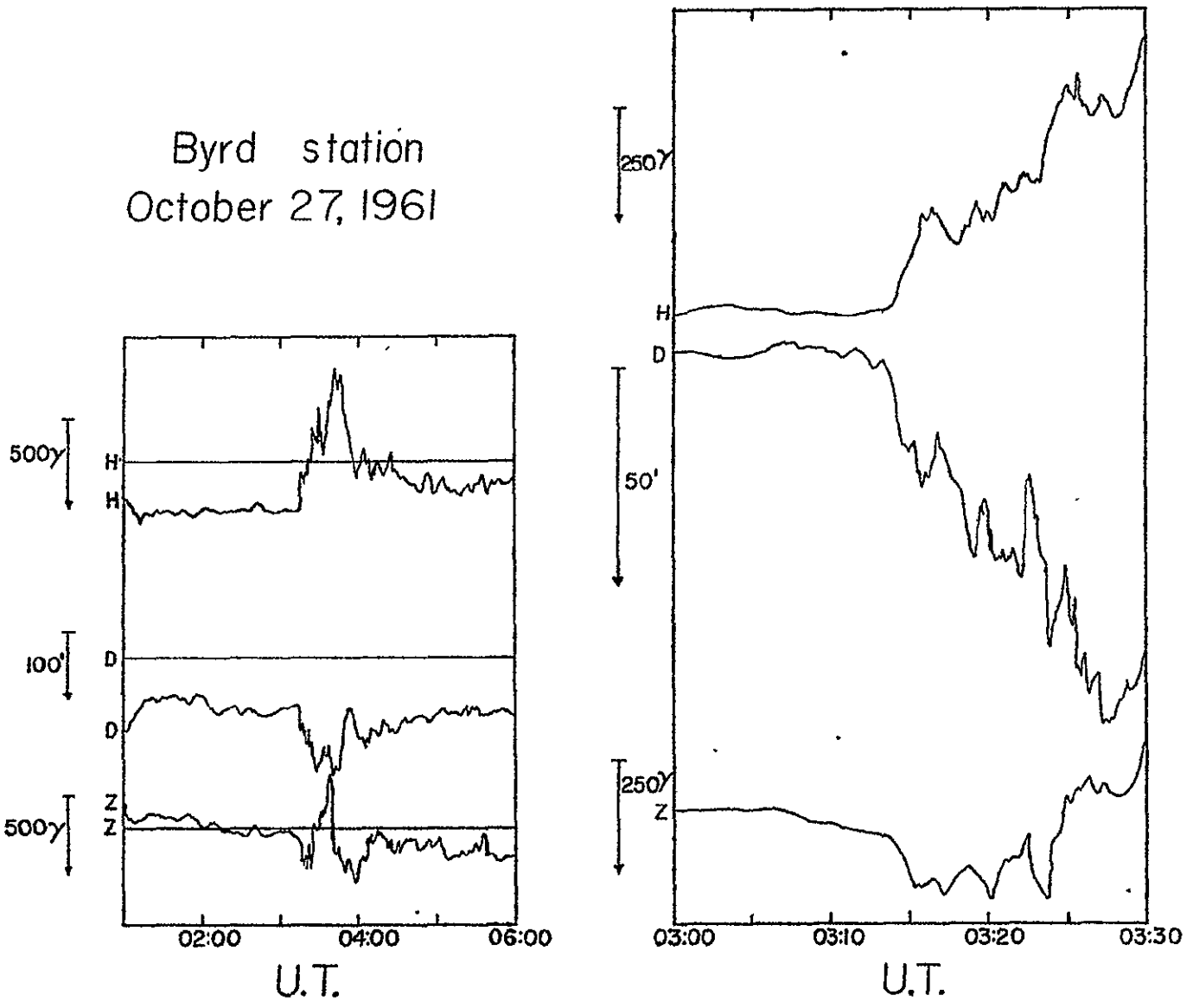

Figure 2

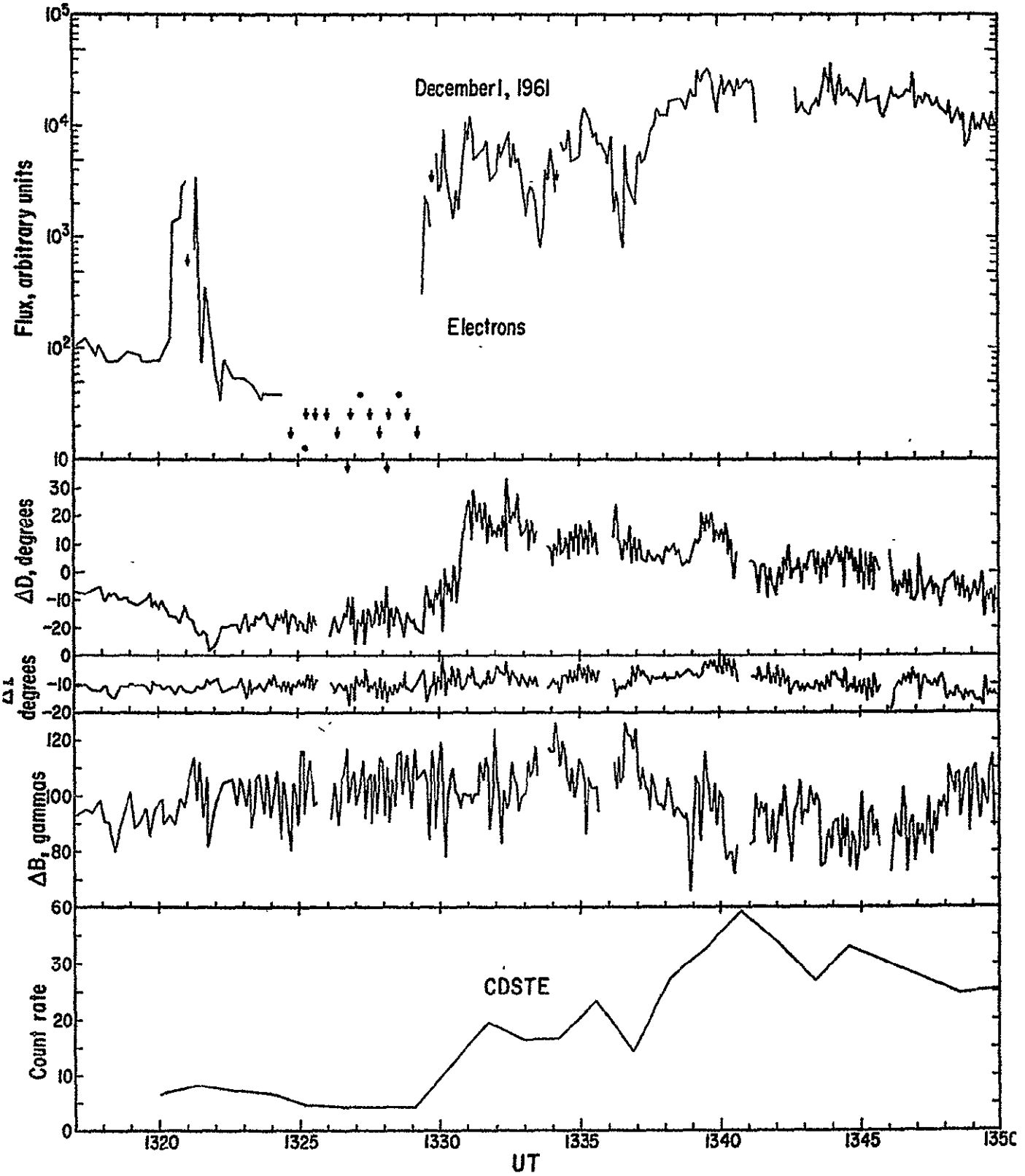
December 1, 1961
Electrons
Flux, arbitrary units
ΔD, degrees
Δ I degrees
ΔB, gammas
Count rate
CDSTE
UT
1320
1325
1330
1335
1340
1345
1350

Figure 3

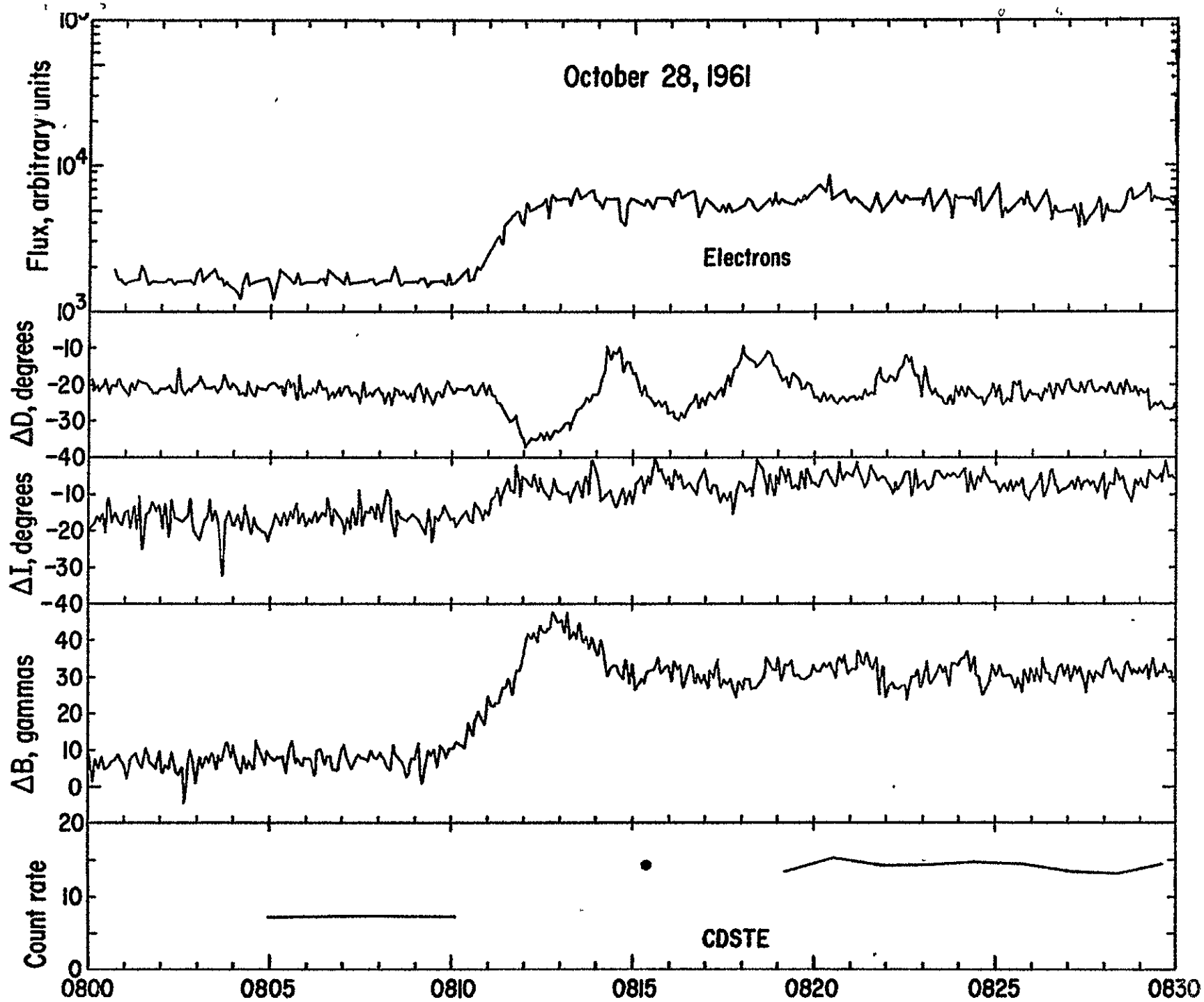

Figure 4

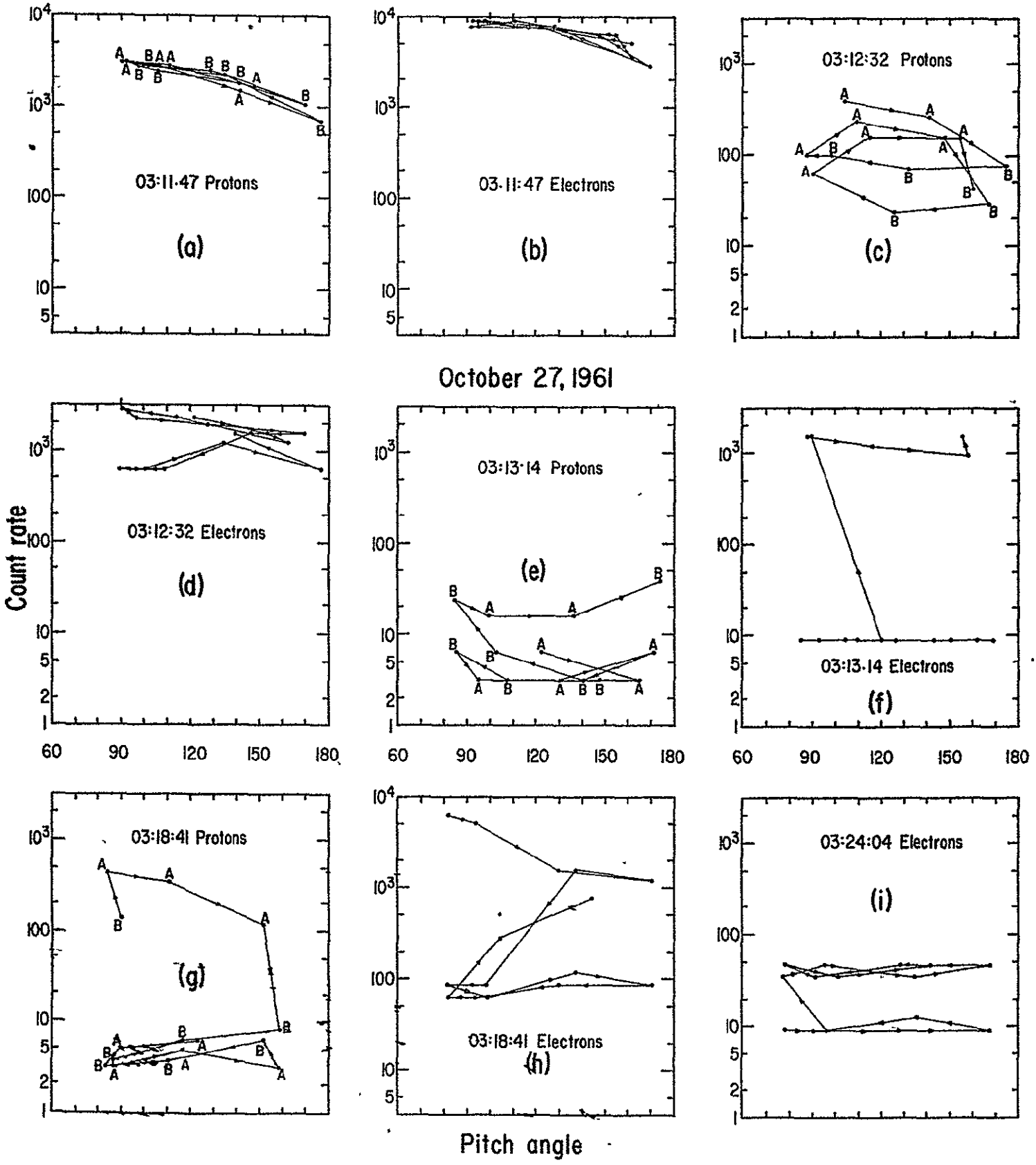
October 27, 1961
03:11:47 Protons
(a)
03:11:47 Electrons
(b)
03:12:32 Protons
(c)
03:12:32 Electrons
(d)
03:13:14 Protons
(e)
03:13:14 Electrons
(f)
03:18:41 Protons
(g)
03:18:41 Electrons
(h)
03:24:04 Electrons
(i)
Count rate
Pitch angle

Figure 5

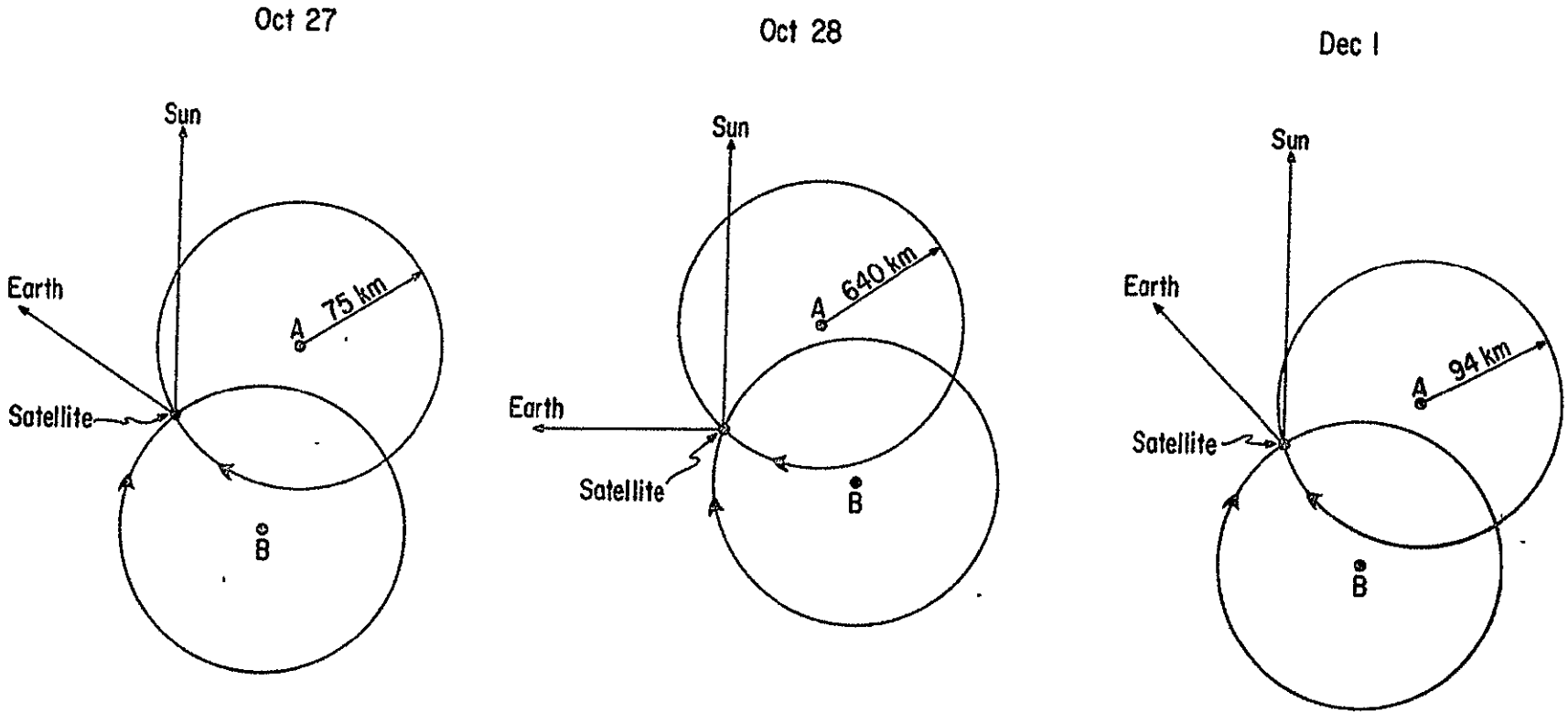
Oct 27
Sun
Earth
Satellite
A
75 km
B
Oct 28
Sun
Earth
Satellite
A
640 km
B
Dec 1
Sun
Earth
Satellite
A
94 km
B

Figure 6

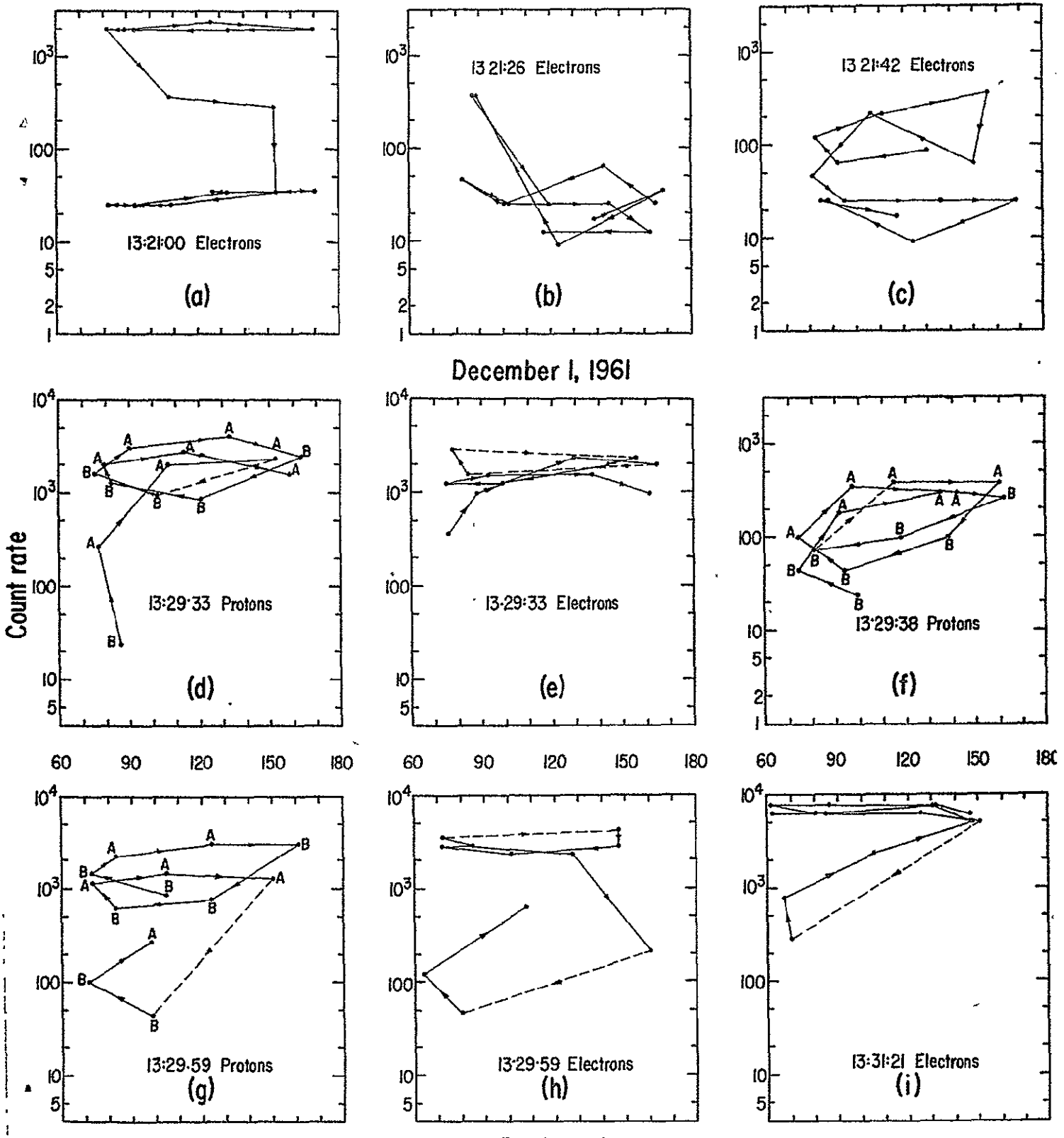
13:21:00 Electrons
(a)
13 21:26 Electrons
(b)
13 21:42 Electrons
(c)
December 1, 1961
13:29:33 Protons
(d)
13:29:33 Electrons
(e)
13:29:38 Protons
(f)
13:29:59 Protons
(g)
13:29:59 Electrons
(h)
13:31:21 Electrons
(i)
Count rate
Pitch angle

Figure 7

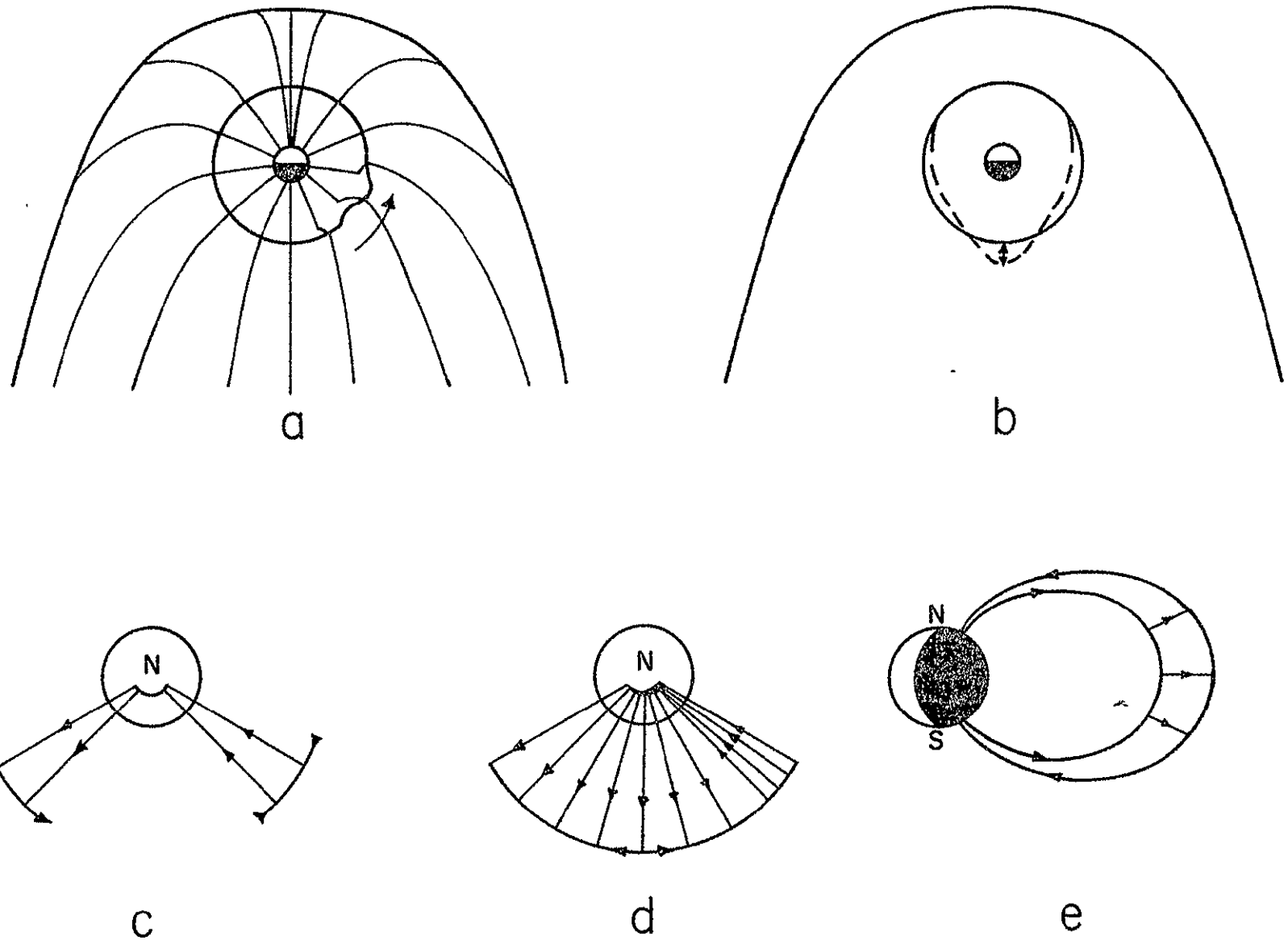

Figure 8